Check for updates

Mechanical and energy absorption properties of 3D-printed honeycomb structures with Voronoi tessellations

Abdelrahman Mohamed Ragab[1], Elsadig Mahdi[1], Kas Oosterhuis[2], Aamir Dean[3] and John-John Cabibihan[1]*

[1]Mechanical and Industrial Engineering Department, Qatar University, Doha, Qatar, [2]ONL Innovation Studio, Netherlands, Netherlands, [3]School of Civil Engineering, Sudan University of Science and Technology, Khartoum, Sudan

3D printing technology is the new frontier in building construction. It is especially useful for making small structures within a short period. Full construction, including interior partitions and exterior façades, can be achieved with this technology. This paper proposes a parametric Voronoi tessellations model for quickly generating and fabricating 3D-printed hexagonal honeycomb partitions for interior design. Comprehensive experimental testing was conducted to characterize the mechanical properties and investigate the energy absorption characteristics of the proposed 3D-printed hexagonal honeycomb while comparing it to alternative hexagonal honeycomb structures. The tests included tensile testing (ASTM-D638) of the printed Polylactic Acid (PLA) material, especially with the almost total absence of conducted research that reported mechanical properties for 3D printed material with low infill percentages such as 10%. In addition, an in-plane quasi-static axial compression testing of the lightweight honeycomb structures was also conducted on the printed structure with the same low infill percentage. Compared to non-Voronoi honeycomb structures, the Voronoi honeycomb resulted in superior mechanical and energy absorption properties with energy absorption values ranging from 350 to 435 J and crash force efficiency being 1.42 to 1.65.

KEYWORDS

honeycomb structures, Voronoi tessellations, 3D printing, PLA, mechanical properties, energy absorption (EA)

1 Introduction

3D printing technology allows the construction of structures to use digital models without using costly and time-consuming manufacturing machines (Parandoush and Lin, 2017). This technology becomes progressively more used for mass customization and the production of various complex designs in the agricultural, healthcare, automotive, aerospace, and civil engineering industries. The 3D printing process deposits materials only where and as needed, making it more sustainable and cost-effective than other manufacturing methods.

Using 3D printing technology to scale up to the level of complete and large structures has to be based on several scheduled innovations in the field of 1) lean parametric design to production processes, saving money, time, and resources; 2) the smart integration of cultural-aesthetic, structural and climatic performance in the 3D printed structures

components; 3) the assembly of prefabricated integrated 3D printed elements into large-scale structures by applying the state-of-the-art principles of mass customization.

Parametric design has already been employed in construction and architecture (Caetano et al., 2020). However, the combination of 3D printing technology with parametric design in building architectural structures has not been exploited yet. This combination allows each building component (such as facades, interior walls, and interior partitions) to have a unique structure and customized finishing pattern, bringing back the visual and tectonic qualities of expert handicrafts of earlier days.

There are a lot of advantages to 3D printing. However, the optimization of the mechanical properties of printed structures, cost, and time could be challenging (Rouf et al., 2022). Hence, the mechanical properties of the 3D printed structures should be investigated and analyzed to investigate their reliability for different manufacturing purposes. Furthermore, many 3D printing parameters, directly and indirectly, affect the mechanical properties of the 3D printed material (Rouf et al., 2022). For instance, increasing the infill density would increase the strength and stiffness, but it would increase the material consumption and cost. Thus, optimization should be considered based on the application and usage of the 3D-printed parts. In addition, material testing, such as tensile tests, would have different results for any minimal change in the settings of the 3D printing parameters (Hsueh et al., 2021).

Besides the tensile properties, many other important properties should be considered while designing 3D printed structures, e.g., the energy absorption capacity and load-carrying capability. Energy absorption characteristics are essential in many applications subjected to compressive loads in various fields, such as civil engineering, aerospace, automotive, and many other technology fields. For example, for buildings or structures, it is desirable and required to have high energy absorption components made from ultra-light material (Ha and Lu, 2020). Those components are supposed to carry a relatively high load in a specified space.

Many researchers have investigated the tensile properties of 3D-printed structures (Johnston and Kazancı, 2021; Santos et al., 2021). It has been found that material properties such as tensile strength, yield strength, and modulus of elasticity change through the 3D printing process by changing infill (density or pattern), layer heights, temperatures, and other printing parameters (Rismalia et al., 2019). Some have studied the effect of the 3D printing parameters on the mechanical properties of printed structures, such as the effect of varying infill density (Seol et al., 2018; Abdullah Aloyaydi et al., 2019; Rismalia et al., 2019; Yeoh et al., 2020; Kamaal et al., 2021), infill pattern (Lubombo and Huneault, 2018; Rismalia et al., 2019; Abeykoon et al., 2020), and layer height (Yao et al., 2019; Kamaal et al., 2021). Generally, infill density has been reported to have a significant effect on the mechanical performance of printed structures (Elmrabet and Siegkas, 2020). Thus, decreasing the infill density would reduce the tensile strength and material stiffness (Farbman and McCoy, 2016; Kamaal et al., 2021). A wide range of infill densities was investigated by various authors and led to different results. For example, some authors suggested that having 80% infill density for PolyLactic Acid (PLA) material would result in maximum stiffness but with more brittleness (Cantrell et al., 2017; Abdullah Aloyaydi et al., 2019; Kamaal

et al., 2021). On the other hand, it has been noted that as the percentage of the infill density increased from 75% to 100%, tensile strength, and elastic modulus would sharply increase by almost double the amount, according to (Seol et al., 2018). It is important to notice that all the previously mentioned studies have investigated only infill percentages from 20% to 100% while neglecting the lower infill densities. Such low infill densities could be desirable in some applications not subjected to high loads, such as facades.

Infill pattern is essential in the 3D printing process, as it significantly affects tensile strength and elastic modulus (Rismalia et al., 2019; Elmrabet and Siegkas, 2020). According to the authors in (Rismalia et al., 2019), the concentric pattern was recommended as it results in higher mechanical properties than other patterns, while the grid or lattice pattern is the second. However, other authors have found that the tensile strength of the grid pattern would be higher than the concentric one (Elmrabet and Siegkas, 2020). Moreover, many infill patterns could choose the optimum pattern depending on the application, weight constraints, and required stiffness. Some patterns would result in higher tensile properties with some specific materials and lower values with other materials (Elmrabet and Siegkas, 2020).

As the ultimate tensile strength of printed PLA would decrease when the layer height increases (becomes thicker) (Chacón et al., 2017; Rajpurohit and Dave, 2019; Yao et al., 2019), another important parameter that affects the mechanical properties is the layer height (Rajpurohit and Dave, 2019). Therefore, having a thinner PLA layer would result in higher tensile strength. Consequently, it would increase the printing time. In addition, another type of material could lead to totally different results. For example, carbon fiber-PLA composite material would increase the tensile strength if the layer height increased, as reported in (Kamaal et al., 2021). Moreover, it was reported by authors in (Kamaal et al., 2021) that reducing the layer height for PLA would have a slight increase in the modulus of elasticity, but it would have a huge effect on the ductility properties. Besides the mechanical properties, the cost and time of the 3D printing process are essential factors to consider for optimization. For instance, increasing infill density would enhance the mechanical properties but require more material, i.e., more cost and time (Abeykoon et al., 2020). Table 1 summarizes and presents the results of previous studies that investigated the tensile properties of 3D printing materials (mainly PLA).

As previously mentioned, energy absorption, load-carrying capacity, and crash efficiency are important characteristics in the design process of many applications (Rajpurohit and Dave, 2019). Like the tensile properties, many authors have investigated the energy absorption characteristics of many different structures (Mahdi et al., 2005; Wang et al., 2011; Mahdi and Hamouda, 2012; Habib et al., 2018; Alkhatib et al., 2020a; Alkhatib et al., 2020b; Alkhatib et al., 2021), among many others.

Wang et al. (2011) investigated experimentally and numerically the energy absorption characteristics of honeycomb structures. Therein, five different geometries of honeycombs were presented; square, triangular, circular, hexagonal, and kagome. The results showed that the kagome honeycomb has the highest value of specific energy absorption, and the hexagonal and triangle structures have the second-highest value for energy absorption capacities and load carrying, with a minimal difference between

TABLE 1 Summary of some previous studies that conducted a tensile test on 3D printed material.

Ref.	Material	Standard Code (Type)	UTS [MPa]	E [MPa]
Elmrabet and Siegkas (2020)	PLA, TPU95A	ISO-527 (1A & 1B), ISO-37:2017 (2)	15.5–72.2	2020–4000
Santos et al. (2021)	PLA	ASTM D638 (Type IV)	50.23	2750
Seol et al. (2018)	PLA	ASTM D638 (Type I)	17.8–50.1	367.7–969.2
Heidari-Rarani et al. (2020)	PLA	ASTM D638 (Type I)	13.88–44.07	1197–3274
Rismalia et al. (2019)	PLA	ASTM D638 (Type I)	28.1–33.3	2760–3280
Kamaal et al. (2021)	Carbon fibre-PLA composite	ASTM D638	25.04–46.26	–
Puteh et al. (2020)	PLA	ASTM D638 (Type IV)	26.4	2300
Rajpurohit and Dave (2019)	PLA	ASTM D638 (Type I)	21.94–47.3	–
Ansari and Kamil (2021)	PLA	ASTM D638 (Type IV)	40.03–59.84	–
Yeoh et al. (2020)	PLA and cPLA	ASTM D638	15.62–23.41	–
Chacón et al. (2017)	PLA	ASTM D638	20.2–89.1	3266–4409

both structures. However, the hexagonal honeycomb possesses higher stability in the stress plateau. Thus, the authors in this study concluded that the hexagonal honeycomb structure has better energy absorption characteristics than the other considered geometries.

In Habib et al. (2018), non-linear numerical simulation has been used to investigate the energy absorption characteristics of nine different honeycomb structures. Similar to the previous study, the hexagonal honeycomb structure resulted in the best energy absorption characteristics compared to the other eight geometries.

Concerning 3D-printed structures, energy absorption characteristics have been studied by many researchers (Habib et al., 2017; Antony et al., 2020; Laban et al., 2021). Many of these studies have considered 3D-printed structures with different geometries and shapes inspired by nature, numerical topology optimization, or parametric design. For example, the authors in Habib et al. (2017) conducted a uniaxial quasi-static compression test on 3D-printed hexagonal honeycomb structures with different wall thicknesses in different orientations and numerical simulations. There were two different considered orientations for the hexagons, one with a flat surface as the top and the other with a corner one as a top. The flat top resulted in higher stability, higher energy absorption values, and a stress plateau (Habib et al., 2017).

Different lattice structures were investigated in Nazir et al. (2022) using a uniaxial compression test to get the energy absorption characteristics while conducting a tensile test as well to get the mechanical properties of that used material. Nazir et al. (2022) concluded that distributing more material near the edge would enhance the energy absorption characteristics, and the square honeycomb configuration has better results than other structures. Nazir et al. (2022) used Multijet Fusion Technology for manufacturing these structures, and this proposed study focuses more on parts that are manufactured using FDM technology.

Li et al. (2023) investigated different PLA printed—Using FDM—Honeycomb structures through an in-plane quasi-static compression test. They (Li et al., 2023) proposed a novel honeycomb design with variable cross-sections showing higher energy absorption properties. A similar investigation was conducted by Sadegh Ebrahimi et al. (2022), and they proposed a re-entrant-star-shaped honeycomb that showed high energy absorption capabilities compared to other designs conducted within the same research.

In Antony et al. (2020), in-plane quasi-static compression and bending tests have been conducted on 3D-printed hexagonal honeycomb structures with different orientations.

The authors in Laban et al. (2021) have recently investigated the load-carrying and energy absorption capacities of four different 3D-printed hexagonal honeycomb geometries. Two additive manufacturing methods have been used, Fused Deposition Modelling (FDM) and Direct Metal Laser Sintering (DMLS). In addition, an in-plane compression test has been used in this study. The results showed that filling the hexagonal honeycomb core with a cross would significantly enhance the load-carrying and energy absorption capacities compared to the coreless hexagonal honeycomb geometry. Moreover, similar collapsing behavior was noticed in structures printed using FDM and DMLS.

Overall, many geometrical optimization studies were devoted to investigating the energy absorption characteristics of different structures (Wang et al., 2011; Mahdi and Hamouda, 2012; Habib et al., 2017; Yang et al., 2018; Antony et al., 2020; Ha and Lu, 2020; Laban et al., 2021; Santos et al., 2021). The previously discussed experimental studies were performed through compression tests conducted on cellular structures such as honeycomb structures (Habib et al., 2017; Yang et al., 2018; Antony et al., 2020; Laban et al., 2021). Furthermore, many of those that discussed comparative studies concluded that the hexagonal honeycomb structure possessed high energy absorption capabilities, high stability, and great compressibility (Wang et al., 2011; Habib et al., 2017) compared to other geometries. Additionally, recent studies

(Laban et al., 2021) showed that increasing a filled hexagonal honeycomb would diminish the energy absorption characteristics. Also, it is important to mention that most of the studies—Mentioned in the literature—That investigated similar energy absorption analysis conducted a tensile test to report the mechanical properties of the utilized material. Furthermore, tensile testing becomes more necessary in this current study especially because of the used low infill percentage.

This paper proposes a parametric Voronoi tessellations model for quickly generating and fabricating 3D-printed hexagonal honeycomb partitions for interior design. Comprehensive experimental testing was conducted to characterize the mechanical properties and investigate the energy absorption characteristics of the proposed 10% infill density 3D-printed Voronoi tessellations hexagonal honeycomb while comparing it to alternative hexagonal honeycomb structures. The testing included tensile testing of the printed Polylactic Acid (PLA) material and in-plane quasi-static axial compression testing of the honeycomb structures.

2 Material and experimental program

The parameterized design and 3D modeling of the honeycomb structures are presented. Next, the 3D printing process and associated printing parameters are discussed. Then, the tensile testing setup for the 3D printing of PolyLactic Acid (PLA) material is presented. Lastly, the experimental setup of the quasi-static axial compression testing will be discussed.

2.1 Proposed design

The proposed structure in this study is formed from similar hexagonal honeycomb blocks filled with Voronoi tessellations arranged in a repeated pattern and attached by magnetic coupling.

2.1.1 Parameterized design and 3D modelling

Parametric modeling involves the development of mathematical relationships between different parameters in the geometric design, along with writing scripts to provide an efficient 3D model, which was then exported as a Standard Tessellation Language (STL) file to proceed with the 3D printing. Herein, parametric modeling was used to create the Voronoi tessellation pattern, which was used to fill the hexagonal honeycomb. Rhino or Rhinoceros 3D software has been utilized for this purpose. The software and the Grasshopper plugin offer powerful tools to create and model complex designs (Fink and Koenig, 2019).

The parametric modeling for the Voronoi tessellations has been carried out through three phases. Figure 1 shows a clustered Grasshopper diagram representing the overall view of the parametric modeling. In the first phase, an enclosed hexagon periphery and generating random points on generated spiral lines were created. In the second phase, the points generated outside the hexagon were removed, and a rectangular boundary was created to generate the Voronoi cells. Finally, a loop function

was initiated to 1) generate the Voronoi cells, 2) use Lloyd's algorithm to have relaxed Voronoi tessellations, and 3) modify the distribution of the cells to optimize the weight of the final design. After creating the hexagonal frame (see Figure 1A), the cluster 'points on spiral lines' was applied following the steps shown in Figure 1B.

Those points were randomly generated from the created spiral curves and eliminated all the points outside the hexagon, resulting in the step shown in Figure 2A. Then, using the Voronoi function, those points were transferred to different Voronoi cells, and a frame was created for each cell to make each one an independent periphery, as shown in Figure 2B.

Inside the loop function and after calling the Voronoi function, the Lloyd's algorithm (see Figure 1C) was utilized to have a new relaxed Voronoi tessellation using the obtained centroid of each cell. After applying 30 iterations in the loop function, the relaxed tessellation shown in Figure 2C was obtained.

To optimize the weight of the final design and allow it to have more strength, the distribution of the Voronoi tessellations was modified using the operation mentioned in Figure 1D. This would push the Voronoi cells to the edges and increase the density of the cells near the edges while reducing it in the center of the hexagon, optimizing the final weight. Figure 3A shows different distributions within different iterations to demonstrate the optimization of the modeling until reaching the convergence state. Finally, the final surface design for the Voronoi tessellations is shown in Figure 3B.

2.1.2 3D model of the hexagonal honeycomb

The 3D Model of the parametric design has been obtained to fit the allowable dimension for a fixed space that would be used to place an interior portion while considering the maximum allowed height for the 3D printer. Figure 4B shows the 3D Model of the final design of a hexagonal honeycomb filled with Voronoi tessellations.

2.1.3 3D magnetic coupling

The hexagonal honeycomb block in Figure 4B was repeated and attached by magnetic coupling to form the proposed structure. Each hexagonal block was attached to the other blocks using the strong N52 neodymium magnets so that the whole structure becomes almost one unit under the applied static loads. In addition, three rectangular slots (magnet slots) have been designed on the front face and another three on the rear face to fit the magnets inside them; see Figures 4C, 5. The slot dimensions are $52 \times 52 \times 7 \ mm^3$ ($l \times w \times h$) to fit correctly with the selected magnets.

2.2 3D printing

The final 3D model of the hexagonal honeycomb was manufactured through Fused Deposition Modelling (FDM)—Or also known as fused filament fabrication (FFF) -, technology. The 3D printing parameters are set as shown in Table 2. This setting was based on minimizing the cost and time required for printing while maintaining the minimum enough strength, as the required application is static. Hence, one hexagonal honeycomb block consumes about 786 g of printing material and takes up to 39 h
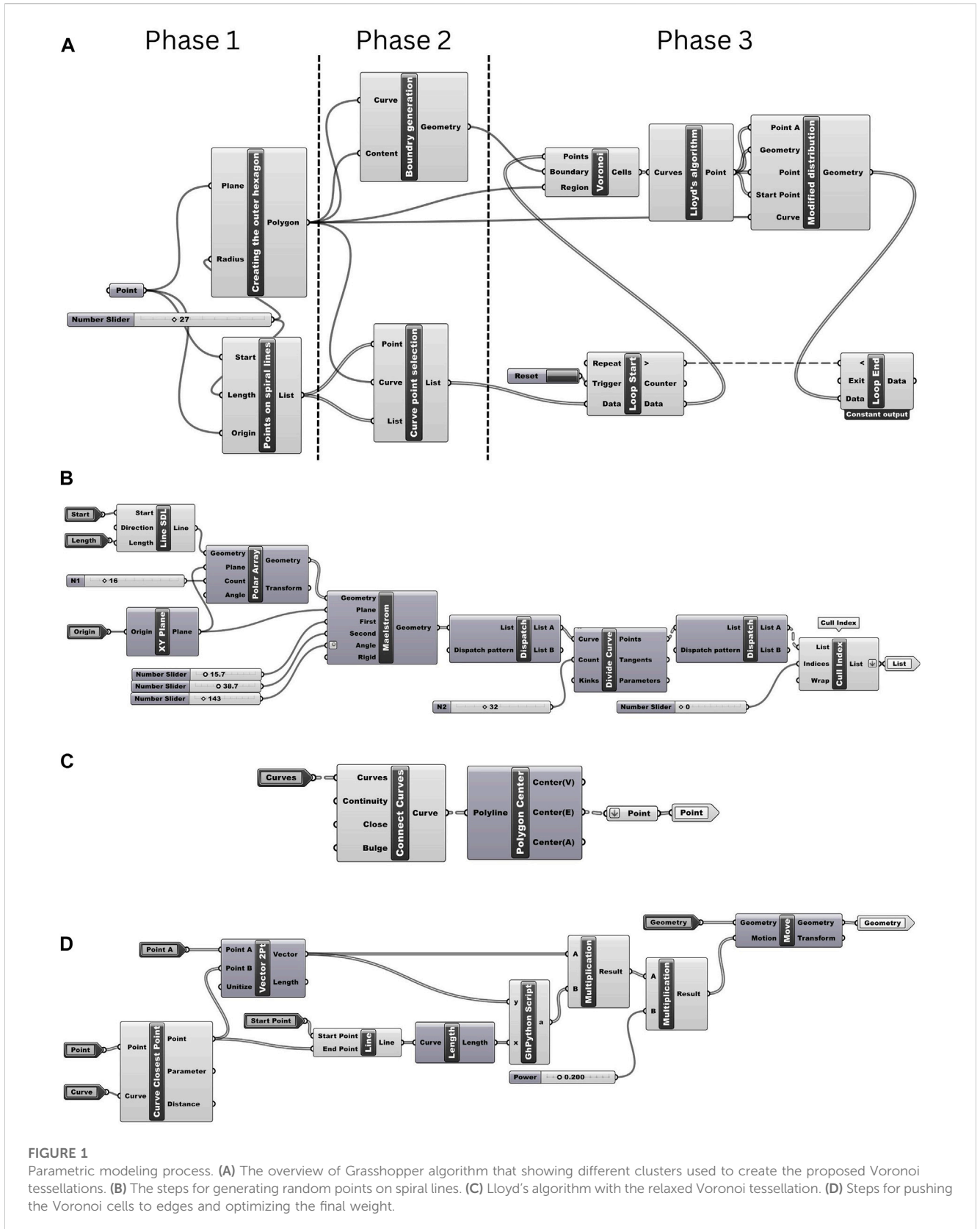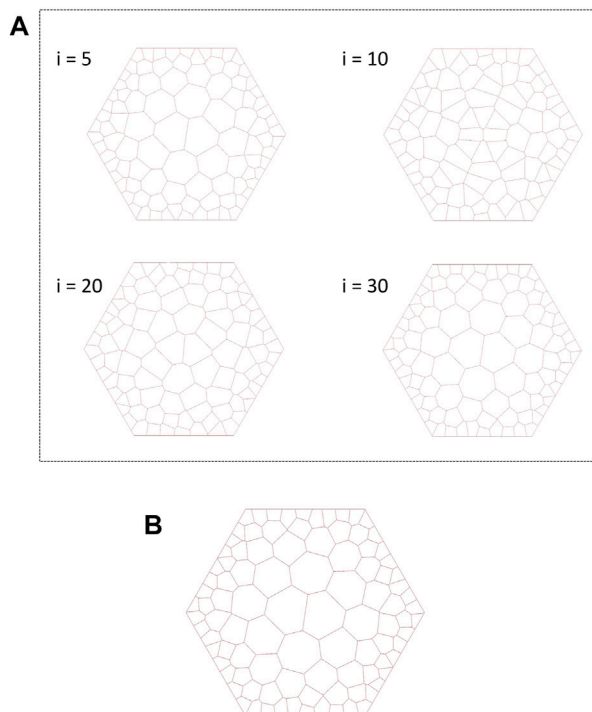
FIGURE 1
Parametric modeling process. **(A)** The overview of Grasshopper algorithm that showing different clusters used to create the proposed Voronoi tessellations. **(B)** The steps for generating random points on spiral lines. **(C)** Lloyd's algorithm with the relaxed Voronoi tessellation. **(D)** Steps for pushing the Voronoi cells to edges and optimizing the final weight.
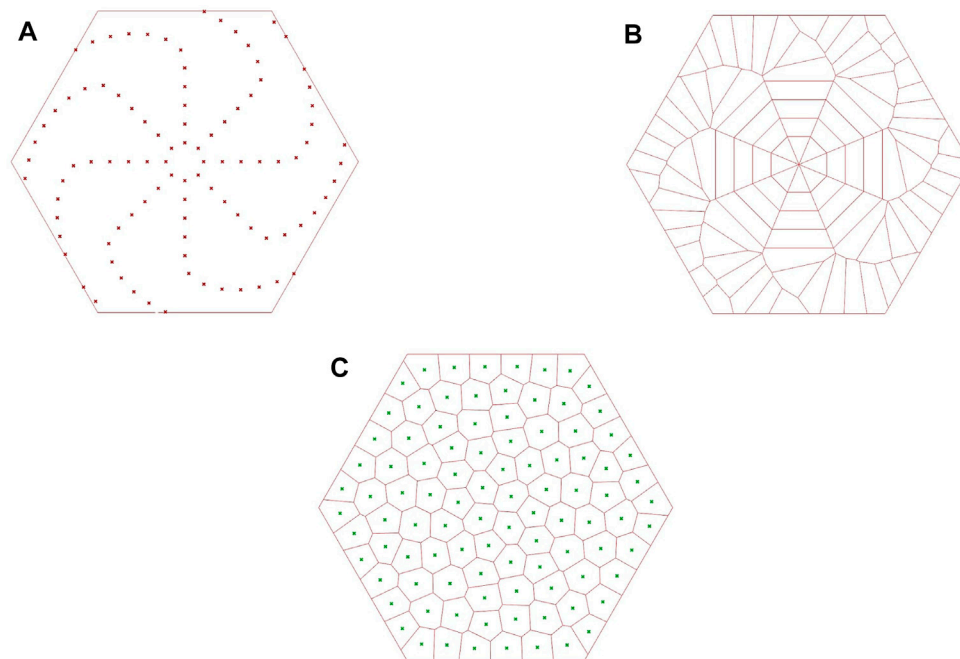
FIGURE 2
Parametric modeling stages. **(A)** Generated random points within the hexagonal frame. **(B)** The initially generated tessellations. **(C)** The relaxed Voronoi tessellation was generated using Lloyd's algorithm.

FIGURE 3
(A) Pushing the Voronoi cells to edges and optimizing the final weight—Modified distribution cluster. **(B)** The Voronoi tessellations' final design is used later to fill the hexagonal honeycomb.

to be printed. PolyLactic Acid (PLA) was used as the printing material. Table 3 shows the general properties of PLA, as reported in Lanzotti et al. (2015).

2.3 Tensile test

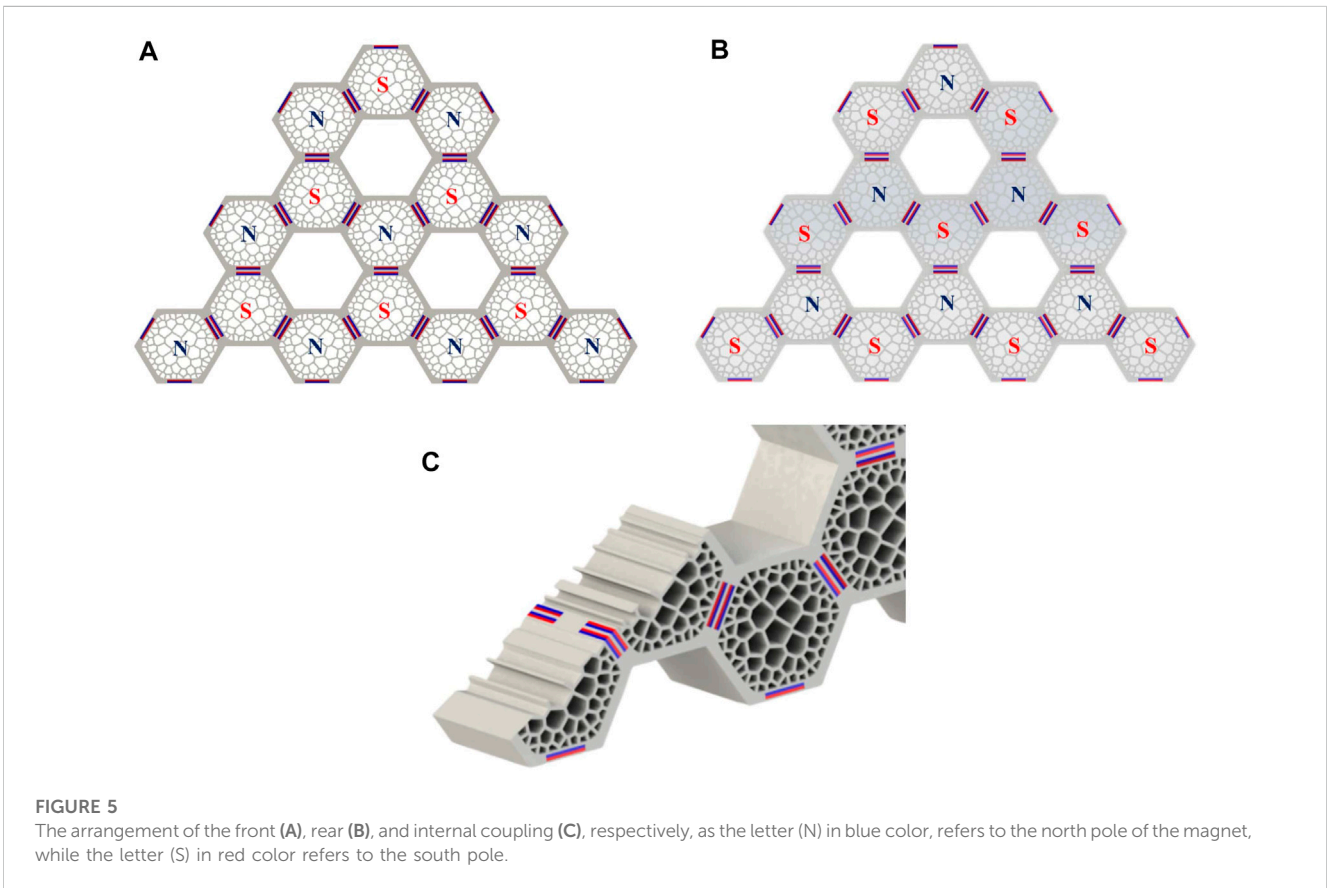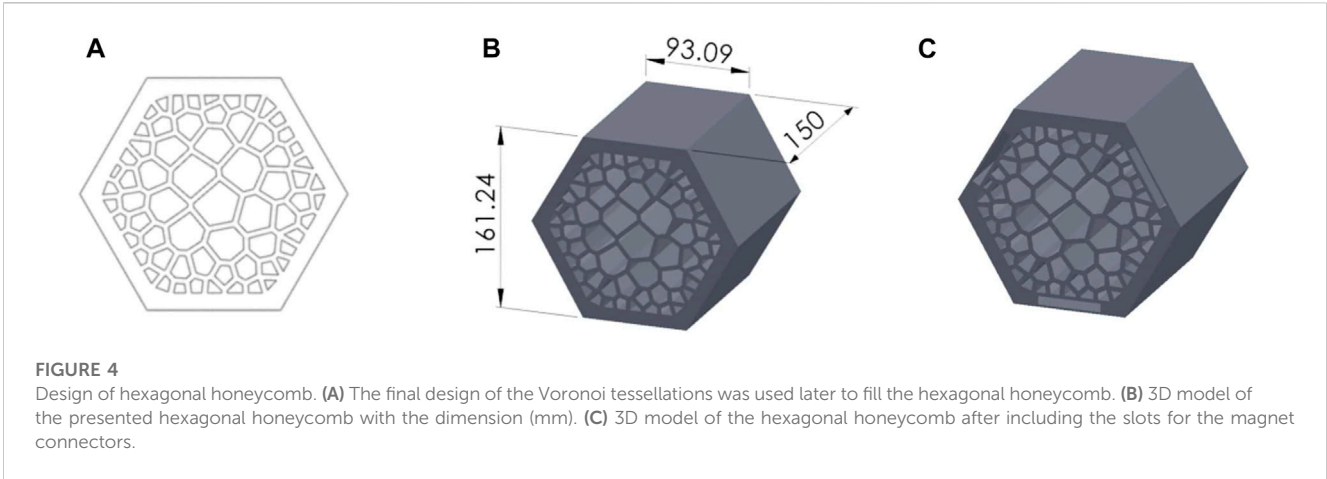### 2.3.1 Preparation of test specimens

Since there is no standard tensile test method for 3D printed polymers, the standard method in (ASTM D638—14) was used as it is the most used standard test method for tensile testing of polymers (see Table 1). For this purpose, a dog bone specimen shape with dimensions similar to the (ASTM D638—14) was utilized. Three test specimens were printed using the QIDI 3D printer using the same PLA material and printing settings used for the honeycomb structure. The weight of the specimens is 8.95 ± 0.015 g.

2.3.2 Test setup

The tensile tests were performed with Instron 5585 Universal Testing Machine. According to ASTM D638—14, the tests were carried out with a constant speed of 5 mm/min inside a closed area, which maintains a temperature of 25°C.

2.3.3 Tensile parameters

The tensile parameters are obtained based on the stress-strain curves obtained from the uniaxial tensile test on the 3D-printed dog-bone specimens. To get the stress and strain values required to plot its curves, the following equations should be considered:

FIGURE 4
Design of hexagonal honeycomb. **(A)** The final design of the Voronoi tessellations was used later to fill the hexagonal honeycomb. **(B)** 3D model of the presented hexagonal honeycomb with the dimension (mm). **(C)** 3D model of the hexagonal honeycomb after including the slots for the magnet connectors.

FIGURE 5
The arrangement of the front **(A)**, rear **(B)**, and internal coupling **(C)**, respectively, as the letter (N) in blue color, refers to the north pole of the magnet, while the letter (S) in red color refers to the south pole.

$$\sigma = \frac{F}{A} \tag{1}$$

$$\varepsilon = \frac{\Delta L}{L_0} \tag{2}$$

where A is the cross-section area of the reduced section in the dog bone shape, F is the applied recorded force, ΔL is the recorded displacement, and L_0 is the length of the reduced section in the dog bone specimens. L_0 is the gauge length with a value of 50 mm, as stated by the ASTM D638—14 (Type I).

2.4 Energy absorption test

2.4.1 Preparation of test specimens

The energy absorption performance of the proposed hexagonal honeycomb structure was investigated through in-plane compressive loading on the prepared experimental samples under quasi-static axial compression. Since the proposed honeycomb structure in Figure 4B consumed a lot of material and time, it was difficult to use the whole part for testing. Hence, only one representative hexagonal honeycomb block was tested.

TABLE 2 Setting of the 3D printing process.

Printing parameter	Setting
Layer height	0.3 mm
Infill pattern	Grid
Infill density	10%
Printing temperature	200°C
Build plate temperature	60°C
Print speed	60 mm/s

TABLE 3 Typical ranges of mechanical properties for PLA material [52].

Mechanical properties	Settings
Tensile modulus of elasticity	2020–3550 MPa
Ultimate tensile strength	14–70 MPa
Yield strength	15.5–72 MPa
Tensile elongation break	0.5%–9.2%
Specific gravity	1.24–1.26 g/cm^3
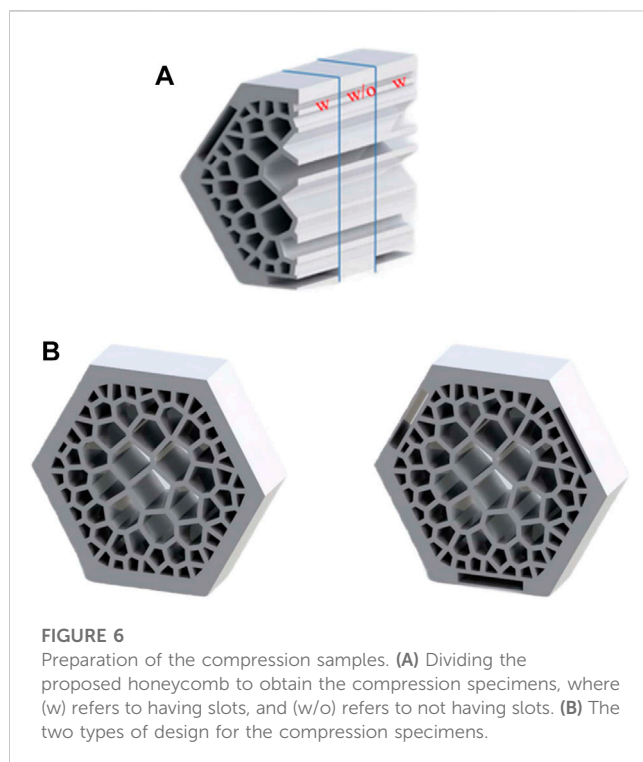
FIGURE 6
Preparation of the compression samples. **(A)** Dividing the proposed honeycomb to obtain the compression specimens, where (w) refers to having slots, and (w/o) refers to not having slots. **(B)** The two types of design for the compression specimens.

The hexagonal honeycomb structures with and without slots were considered in the analysis (Figure 6). Furthermore, alternative designs were also considered to have a comparative study between the proposed design and other designs. Finally, all the designs have the same outer thickness and depth, as shown in Supplementary Figure S1 (Supplementary Material). A total of thirty specimens were 3D printed (three for each case), as shown in Figure 7, and the weights of specimens were presented in the same Figure 7.

2.4.2 Test setup

The 3D printed specimens were subjected to in-plane compressive loading to investigate the performance of energy absorption characteristics and load-carrying capability. The in-plane compressive loading was applied by the testing machine with a constant speed of 15 mm/min following the ASTM E9-09 specifications [Supplementary Figure S2 (Supplementary Material)].

The load-displacement data were recorded every 1 ms, and the crushing behavior of all designs was video recorded with a quality of 1080 p HD at 60 frames per second.

2.4.3 Energy absorption parameters

The energy absorption (crashworthiness) parameters were calculated based on the load-displacement curves obtained from the in-plane compressive loading test on the 3D-printed specimens. Initial peak load (Pp) and mean force (Pm) were obtained directly from the curves. Crush force efficiency (CFE), energy absorbed (EA), and specific energy absorbed (SEA) were calculated as follows, respectively:

$$CFE = \frac{P_p}{P_m} \tag{3}$$

$$EA = \int_0^\delta P \, d\delta \tag{4}$$

$$SEA = \frac{EA}{weight} \tag{5}$$

3 Results and discussion

The experimental results are reported and discussed. First, the tensile testing results on the 3D-printed PLA material dog-bone specimens are presented and discussed. Then, the experimental results of the quasi-static axial compression tests on the hexagonal honeycomb structures are outlined and discussed.

3.1 Tensile test

The stress-strain curves are shown in Figure 8A for the three specimens. These curves were derived from the recorded load-displacement data using Eqs 1, 2. Accordingly, the ultimate tensile strength (σ_t) at a specific strain (ε_t) and the modulus of elasticity (with the help of linear regression) were calculated for the three specimens. The obtained values for ultimate tensile strength are 41.54 ± 2.02 MPa, and for modulus of elasticity is 1003.95 ± 11.09 MPa, and both are within some of the reported ranges in the literature. Additionally, the value of strain (ε_t) at (σ_t) is 0.06 ± 0.004. The differences are attributed to each study's different 3D printing settings. However, the presented values in this study are significantly important as a lack of studies investigating such a low infill percentage of 10%. Figure 8B shows the three test specimens after a fracture.

3.2 Energy absorption test

Ten designs of hexagonal honeycomb were investigated under quasi-static in-plane compression, five with magnet slots and five
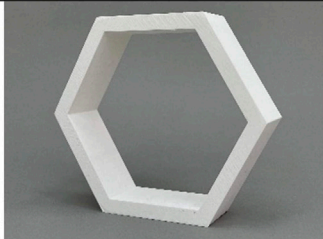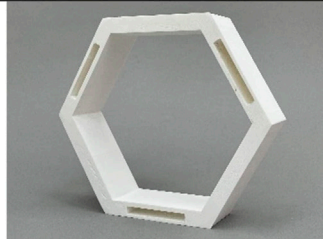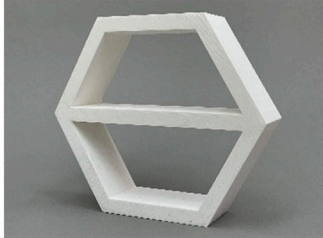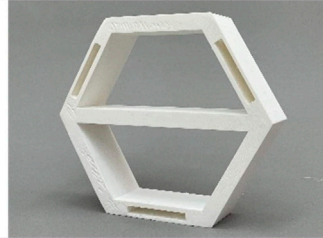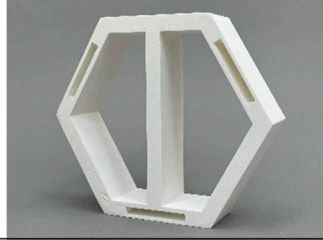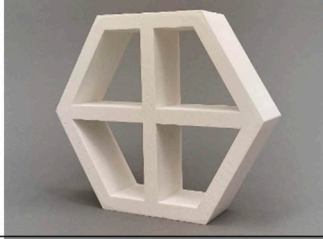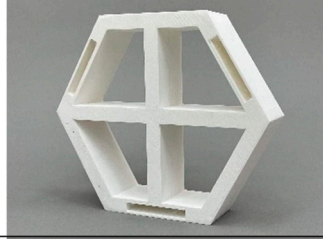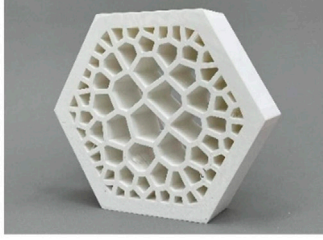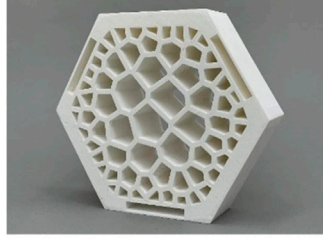
FIGURE 7
3D-printed sample from each group, also the average weight of each group is mentioned in (g).

without. From each design, three specimens were 3D printed and tested.

For each specimen, the load-displacement data were recorded and used to plot the load-displacement curve (Figure 9). Those curves were used to calculate the energy absorption parameters discussed earlier (Table 4) using Eqs 3–5. A series of figures of the deformed configuration of all ten designs retraces the crushing process and behavior under quasi-static in-plane compression at different selected configurations (timeframes) [Su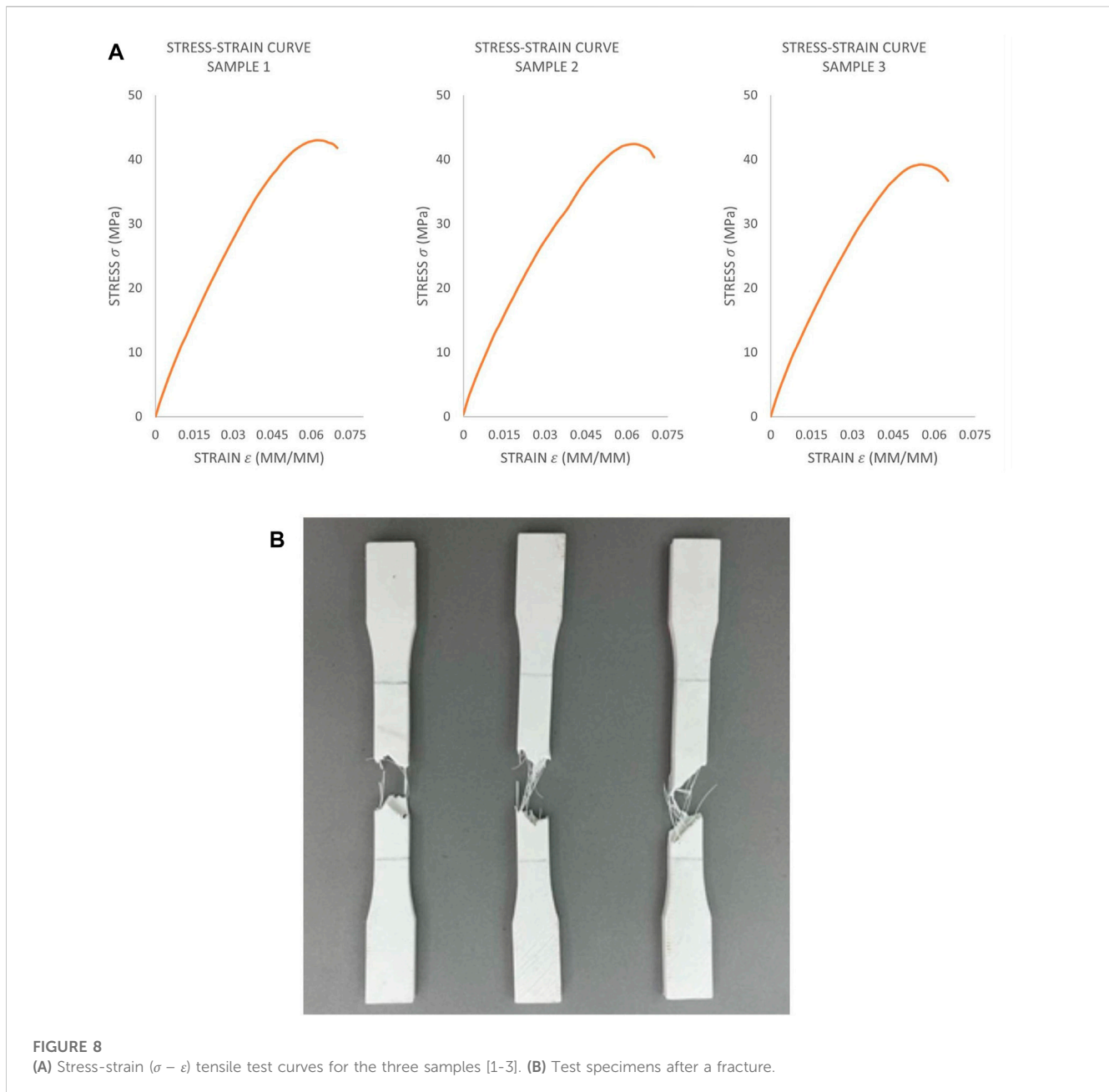pplementary Figure S3 (Supplementary Material)]. The amount of absorbed energy for each design group and the corresponding specific energy absorption values are summarized in Table 4. From those results, it can be seen that the hexagonal honeycomb structures with Voronoi tessellations (i.e., Group

J and E) have the highest energy absorption capacities compared to the other designs with and without slots. Furthermore, Group J has higher energy absorption than Group E due to the existence of slots in Group J. However, the influence of the existence of slots is discussed in more detail later in this section. Additionally, the coreless design (Groups A and F) has the lowest energy absorption in both with/without slots designs. Furthermore, the column (Group C) and cross (Group D) designs without slots have very close absorbed energy values. However, including slots allows the column design (Group H) to have a higher mean absorbed energy than the cross one (Group I).

The specified energy absorption parameter (SEA) resulted in almost the same behavior as the energy absorption. The column design (Group C and H) shows higher SEA values than the heavier

FIGURE 8
(A) Stress-strain ($\sigma - \varepsilon$) tensile test curves for the three samples [1-3]. **(B)** Test specimens after a fracture.

cross design (Group D and I) in both with/without slots design. This unexpected behavior of the cross design could be explained by its crushing behavior [Supplementary Figure S3 (Supplementary Material)], as there was a stress concentration located in the middle intersection (Figure 10A), that caused it to break in the early stage of the crushing process.

Another important energy absorption performance parameter is the initial peak load (P_p), as explained in Section 3. The values of the initial peak load for each design group are shown in Table 4. The hexagonal honeycombs with Voronoi tessellations (Group E and J) resulted in the highest P_p values compared to other designs.

The P_p values were then used to calculate the crushing force efficiency (CFE) through Eq. 3. The mean load (P_m) and CFE values are tabulated in Table 4. Again, Group E and J show the

highest CFE values, indicating the stability of the honeycomb design filled with Voronoi tessellations in carrying the load during the compression test.

Figure 10 shows the scanning electron microscopy photographs taken for the Group J design. The scanned region was the first Voronoi cell that experienced a deformation. The same location was scanned before (Figure 10B) and after (Figure 10C) the crushing process. It is clear that the printed layers got separated and deformed due to the compressive load.

Next, the influence of the existence of slots is discussed in more detail. As shown in Figure 11A, the Voronoi tessellations honeycomb with slots design has more than four times the absorbed energy compared to the cross and column designs. However, the amount of absorbed energy for cross and column with/without slots designs is very
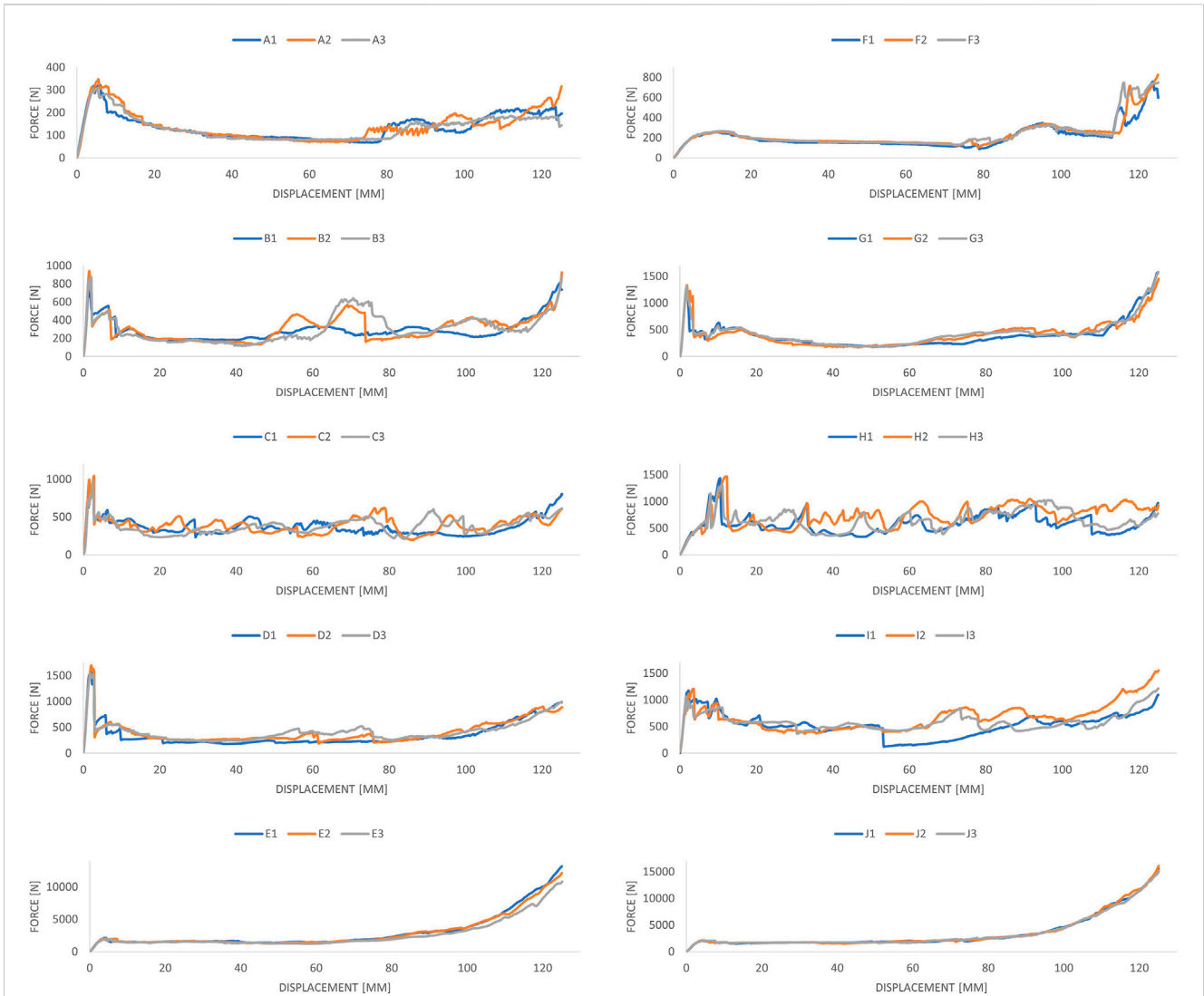
FIGURE 9
Force and displacement curves for all groups and samples. The graph legends represent the label of each sample.

TABLE 4 Experimental initial peak force, average of applied forces, crash force efficiency, energy absorption, and specific energy absorption results for each group.

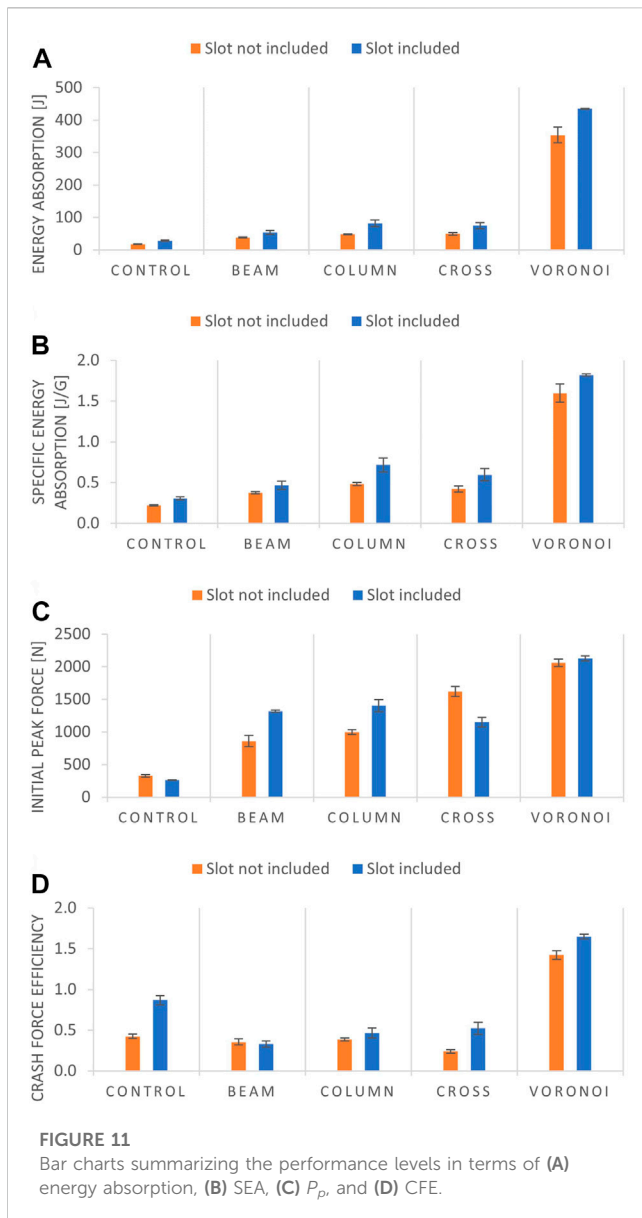| Groups	Initial peak force [N]	Average force [N]	Crash force efficiency (CFE)	Energy absorption [J]	Specific energy absorption [J/g]
Group A	325.690 ± 4.228	138.263 ± 1.169	0.425 ± 0.028	17.289 ± 0.498	0.222 ± 0.008
Group B	858.035 ± 5.387	304.983 ± 0.355	0.355 ± 0.039	37.991 ± 1.404	0.376 ± 0.014
Group C	996.841 ± 3.208	382.977 ± 0.384	0.384 ± 0.020	47.845 ± 1.530	0.484 ± 0.018
Group D	1620.558 ± 6.169	386.357 ± 0.238	0.238 ± 0.020	49.072 ± 2.271	0.421 ± 0.017
Group E	2059.029 ± 5.466	2924.783 ± 0.420	1.420 ± 0.054	353.777 ± 4.722	1.597 ± 0.012
Group F	261.557 ± 3.793	227.340 ± 0.869	0.869 ± 0.056	28.304 ± 1.724	0.306 ± 0.019
Group G	1317.756 ± 4.433	435.509 ± 0.330	0.330 ± 0.036	54.170 ± 1.851	0.465 ± 0.010
Group H	1401.253 ± 5.497	654.409 ± 0.467	0.467 ± 0.063	81.828 ± 2.640	0.715 ± 0.034
Group I	1148.820 ± 4.822	599.101 ± 0.521	0.521 ± 0.074	74.781 ± 3.424	0.595 ± 0.015
Group J	2623.791 ± 6.613	3501.956 ± 3.031	1.649 ± 0.029	434.681 ± 2.424	1.819 ± 0.001
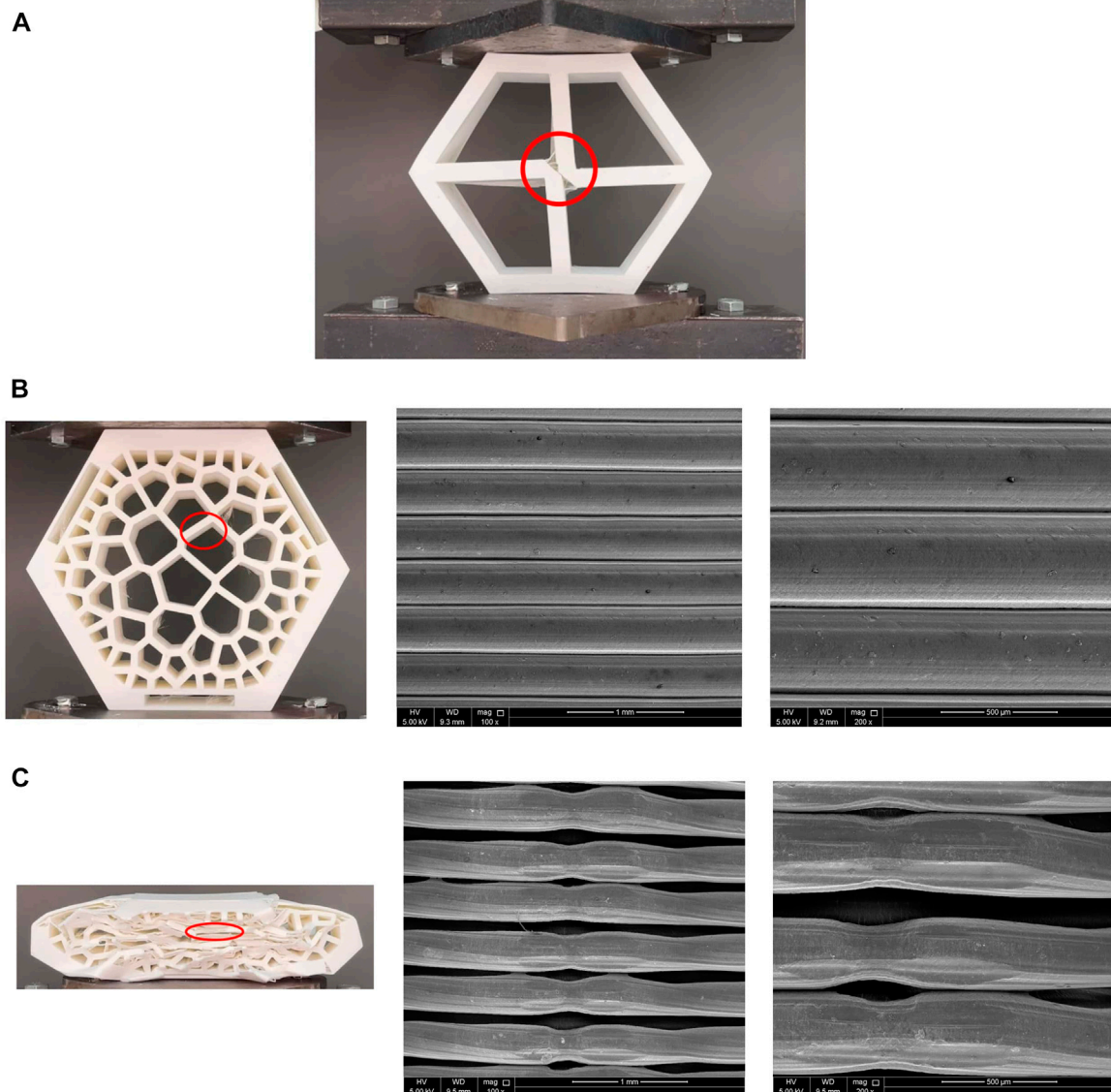
FIGURE 10
(A) The crushing process of one sample from Group D. Also, scanning electron microscopy photographs highlighting the defects at the first deformed Voronoi cell while showing **(B)** the pre-compression and **(C)** the final deformed cases.

close. The column has a slightly higher value than the cross design when the slots are included. Furthermore, Figure 11A shows a general trend that included slots in the designs has significantly increased the amount of absorbed energy for all designs compared to designs with no slots.

In Figure 11B, the specified energy absorption was compared. Similar to the absorbed energy results, all the designs with slots resulted in higher SEA values than their correspondence designs without slots. The cross design (higher weight) resulted in less SEA value than the column design, as discussed and explained earlier. The existence of the slots allows the column configuration to have more than a 16% SEA increase than the cross one when comp. Additionally, among the designs with slots, the Voronoi tessellations design has more SEA than the column design (which is the second-highest SEA value) by 60% and by 70% for the designs without slots. Furthermore, the difference between the slots and without slots designs for Voronoi tessellation design is only 12%.

Figures 11C, D compare the results obtained for the initial peak load and rush force efficiency, respectively. The values of Pm for Voronoi tessellations design with/without slots are very close, with only a 3% difference. However, the previously made conclusions regarding the trend of energy absorption and specified energy absorption do not hold here. For instance, the cross design without slots has a significantly higher Pm than the one when slots are included. One likely explanation is that adding slots in the cross design would increase the stress concentration around the slots' corners, easing the crushing process. Hence, decreasing the Pm would decrease the load required to initiate a permanent deformation (crushing or breaking) in the structure. This conclusion made can be supported by the crushing process of Group I in Supplementary Figure S3 (Supplementary Material). Additionally, among the designs without slots, and in contrast to EA and SEA, the cross design has a higher value of Pm than the column one. This could be explained as that during the crushing process of the cross design,

FIGURE 11
Bar charts summarizing the performance levels in terms of **(A)** energy absorption, **(B)** SEA, **(C)** P_p, and **(D)** CFE.

4 Conclusion and outlook

This paper addresses a comparative investigation of the energy absorption performance of 3D-printed hexagonal honeycomb structures with different infillings. Additionally, a tensile test has been conducted to characterize the 10% infill density 3D printed PLA material for the mechanical properties to fill the gap in the literature. A honeycomb structure filled with Voronoi tessellations resulted in the highest EA, SEA, P_m, and CFE values, while slots in its design increased the energy absorption performance even more. Hence, the proposed Voronoi design provides superior mechanical and energy absorption performance compared to the non-Voronoi counter-parts, with energy absorption values ranging from 350 J to 435 J and crash force efficiency being 1.42 to 1.65. It is noteworthy that all of the designs have been 3D printed with an infill density of 10%, making these structures very light to save material and time while providing good energy absorption properties. For future work, this study could be expanded to cover some of the current study's limitations, such as the slow printing time, layers delamination, and various material testing. Moreover, different printing materials and different printing settings could be used. For instance, investigating how the tensile and energy absorption properties would differ if different infill patterns, materials, layer heights, or other 3D printing factors were used. Furthermore, the performance of the proposed Voronoi design could be also investigated under dynamic loading.

Data availability statement

The original contributions presented in the study are included in the article/Supplementary Material, further inquiries can be directed to the corresponding author.

Author contributions

Conceptualization, J-JC, KO, and AR; methodology, J-JC, KO, AR, and EM; software, AR; validation, J-JC; formal analysis, AR, EM, and J-JC; data curation, AR; writing—Original draft preparation, AR; writing—Review and editing, J-JC, EM, AR, and AD; visualization, AR and AD; supervision, J-JC, KO, and EM; project administration, J-JC; funding acquisition, J-JC and KO. All authors contributed to the article and approved the submitted version.

high force is required to overcome the intersection point (Figure 10A) to initiate the permanent deformation. After breaking this point, there is no other significant core support, meaning less force would be required to continue the crushing process. Thus, the total area under the force-displacement curve would decrease, which means decreasing the energy absorption and SEA, see Figure 9. Figure 11D shows a general trend of increased CFE values for the designs with slots. However, the beam configuration when slots are included has a slightly higher CFE than those without slots by only 7%. Moreover, in all design cases, the coreless (control) designs with/without slots have the second-highest CFE values, which reflects the structure's high stability in carrying the load during the crushing process. Furthermore, among the designs with slots, the Voronoi tessellations have more CFE value than the coreless one by 47% and 70% for the case without slots. According to Laban et al. (2021), among the cross, column, beam, and coreless designs, the cross design has the highest P_m and SEA values and the lowest CFE. However, the coreless control design has the highest CFE value, and the proposed Voronoi design has the highest SEA, P_m, and CFE values.

Conflict of interest

The authors declare that the research was conducted in the absence of any commercial or financial relationships that could be construed as a potential conflict of interest.

Publisher's note

All claims expressed in this article are solely those of the authors and do not necessarily represent those of their affiliated organizations, or those of the publisher, the editors and the reviewers. Any product that may be evaluated in this article, or claim that may be made by its manufacturer, is not guaranteed or endorsed by the publisher.

Supplementary material

The Supplementary Material for this article can be found online at: https://www.frontiersin.org/articles/10.3389/fmech.2023.1204893/full#supplementary-material

References

Abdullah Aloyaydi, B., Sivasankaran, S., and Rizk Ammar, H. (2019). Influence of infill density on microstructure and flexural behavior of 3D printed PLA thermoplastic parts processed by fusion deposition modeling. *AIMS Mater. Sci.* 6, 1033–1048.

Abeykoon, C., Sri-Amphorn, P., and Fernando, A. (2020). Optimization of fused deposition modeling parameters for improved PLA and ABS 3D printed structures. *Int. J. Lightweight Mater. Manuf.* 3, 284–297.

Alkhatib, F., Mahdi, E., and Dean, A. (2020a). Crushing response of cfrp and kfrp composite corrugated tubes to quasi-static slipping axial loading: Experimental investigation and numerical simulation. *Compos. Struct.* 246, 112370. doi:10.1016/j.compstruct.2020.112370

Alkhatib, F., Mahdi, E., and Dean, A. (2021). Design and evaluation of hybrid composite plates for ballistic protection: Experimental and numerical investigations. *Polymers* 13. doi:10.3390/polym13091450

Alkhatib, F., Mahdi, E., and Dean, A. (2020b). Development of composite double-hat energy absorber device subjected to traverser loads. *Compos. Struct.* 240, 112046. doi:10.1016/j.compstruct.2020.112046

Ansari, A. A., and Kamil, M. (2021). Effect of print speed and extrusion temperature on properties of 3D printed PLA using fused deposition modeling process. *Mater. Today Proc.* 45, 5462–5468.

Antony, S., Cherouat, A., and Montay, G. (2020). Fabrication and characterization of hemp fibre based 3D printed honeycomb sandwich structure by FDM process. *Appl. Compos. Mater.* 27, 935–953.

Caetano, I., Santos, L., and Leitão, A. (2020). Computational design in architecture: Defining parametric, generative, and algorithmic design. *Front. Archit. Res.* 9, 287–300. doi:10.1016/j.foar.2019.12.008

Cantrell, J. T., Rohde, S., Damiani, D., Gurnani, R., DiSandro, L., Anton, J., et al. (2017). Experimental characterization of the mechanical properties of 3D-printed ABS and polycarbonate parts. *Rapid Prototyp. J.* 23, 811–824.

Chacón, J., Caminero, M., García-Plaza, E., and Núñez, P. (2017). Additive manufacturing of PLA structures using fused deposition modelling: Effect of process parameters on mechanical properties and their optimal selection. *Mater. Des.* 124, 143–157.

Elmrabet, N., and Siegkas, P. (2020). Dimensional considerations on the mechanical properties of 3D printed polymer parts. *Polym. Test.* 90, 106656.

Farbman, D., and McCoy, C. (2016). "Materials testing of 3D printed ABS and PLA samples to guide mechanical design," in *Materials; biomanufacturing; properties, applications and systems; sustainable manufacturing* (American Society of Mechanical Engineers), 2. doi:10.1115/MSEC2016-8668

Fink, T., and Koenig, R. (2019). Integrated parametric urban design in grasshopper/Rhinoceros 3D—Demonstrated on a master plan in vienna. *Proc. 37th eCAADe 23rd SIGraDi Conf.*, 313–322. doi:10.52842/conf.ecaade.2019.3.313

Ha, N. S., and Lu, G. (2020). A review of recent research on bio-inspired structures and materials for energy absorption applications. *Compos. Part B Eng.* 181, 107496. doi:10.1016/j.compositesb.2019.107496

Habib, F. N., Iovenitti, P., Masood, S. H., and Nikzad, M. (2018). Cell geometry effect on in-plane energy absorption of periodic honeycomb structures. *Int. J. Adv. Manuf. Technol.* 94, 2369–2380.

Habib, F. N., Iovenitti, P., Masood, S. H., and Nikzad, M. (2017). In-plane energy absorption evaluation of 3D printed polymeric honeycombs. *Virtual Phys. Prototyp.* 12, 117–131.

Heidari-Rarani, M., Sadeghi, P., and Ezati, N. (2020). Effect of processing parameters on tensile properties of fdm 3d printed of pla specimens. *J. Sci. Technol. Compos.* 7, 855–862.

Hsueh, M.-H., Lai, C.-J., Chung, C.-F., Wang, S.-H., Huang, W.-C., Pan, C.-Y., et al. (2021). Effect of printing parameters on the tensile properties of 3d-printed polylactic acid (pla) based on fused deposition modeling. *Polymers* 13. doi:10.3390/polym13142387

Johnston, R., and Kazancı, Z. (2021). Analysis of additively manufactured (3D printed) dual-material auxetic structures under compression. *Addit. Manuf.* 38, 101783.

Kamaal, M., Anas, M., Rastogi, H., Bhardwaj, N., and Rahaman, A. (2021). Effect of FDM process parameters on mechanical properties of 3D-printed carbon fibre–PLA composite. *Prog. Addit. Manuf.* 6, 63–69.

Laban, O., Mahdi, E., Samim, S., and Cabibihan, J.-J. (2021). A comparative study between polymer and metal additive manufacturing approaches in investigating stiffened hexagonal cells. *Materials* 14.

Lanzotti, A., Grasso, M., Staiano, G., and Martorelli, M. (2015). The impact of process parameters on mechanical properties of parts fabricated in PLA with an open-source 3-D printer. *Rapid Prototyp. J.* 21, 604–617.

Li, T., Sun, J., Leng, J., and Liu, Y. (2023). Quasi-static compressive behavior and energy absorption of novel cellular structures with varying cross-section dimension. *Compos. Struct.* 306, 116582. doi:10.1016/j.compstruct.2022.116582

Lubombo, C., and Huneault, M. (2018). Effect of infill patterns on the mechanical performance of lightweight 3D-printed cellular PLA parts. *Mater. today Commun.* 17, 214–228.

Mahdi, E., and Hamouda, A. (2012). Energy absorption capability of composite hexagonal ring systems. *Mater. Des.* 34, 201–210. doi:10.1016/j.matdes.2011.07.070

Mahdi, E., Hamouda, A., Mokhtar, A., and Majid, D. (2005). Many aspects to improve damage tolerance of collapsible composite energy absorber devices. *Compos. Struct.* 67, 175–187. doi:10.1016/j.compstruct.2004.09.010

Nazir, A., Arshad, A. B., Lin, S.-C., and Jeng, J.-Y. (2022). Mechanical performance of lightweight-designed honeycomb structures fabricated using multijet fusion additive manufacturing technology. *3D Print. Addit. Manuf.* 9, 311–325. doi:10.1089/3dp.2021.0004

Parandoush, P., and Lin, D. (2017). A review on additive manufacturing of polymer-fiber composites. *Compos. Struct.* 182, 36–53.

Puteh, K. A. W. Z., Wan Muhamad, W. M., and Irfan, A. R. (2020). Computational modelling and characterization of stress concentration of line pattern at various angle orientation for cyclic loading. *PalArch's J. Archaeol. Egypt/Egyptol.* 17, 4068–4084.

Rajpurohit, S. R., and Dave, H. K. (2019). Analysis of tensile strength of a fused filament fabricated PLA part using an open-source 3D printer. *Int. J. Adv. Manuf. Technol.*, 1525–1536.

Rismalia, M., Hidajat, S. C., Permana, I. G. R., Hadisujoto, B., Muslimin, M., and Triawan, F. (2019). Infill pattern and density effects on the tensile properties of 3D printed PLA material. *J. Phys. Conf. Ser.* 1402, 044041.

Rouf, S., Raina, A., Irfan Ul Haq, M., Naveed, N., Jeganmohan, S., and Farzana Kichloo, A. (2022). 3d printed parts and mechanical properties: Influencing parameters, sustainability aspects, global market scenario, challenges and applications. *Adv. Industrial Eng. Polym. Res.* 5, 143–158. doi:10.1016/j.aiepr.2022.02.001

Sadegh Ebrahimi, M., Hashemi, R., and Etemadi, E. (2022). In-plane energy absorption characteristics and mechanical properties of 3d printed novel hybrid cellular structures. *J. Mater. Res. Technol.* 20, 3616–3632. doi:10.1016/j.jmrt.2022.08.064

Santos, F. A., Rebelo, H., Coutinho, M., Sutherland, L. S., Cismasiu, C., Farina, I., et al. (2021). Low velocity impact response of 3D printed structures formed by cellular metamaterials and stiffening plates: PLA vs. PETg. Compos. Struct. 256, 113128.

Seol, K.-S., Zhao, P., Shin, B.-C., and Zhang, S.-U. (2018). Infill print parameters for mechanical properties of 3D printed PLA parts. *Korean Soc. Manuf. Process Eng.* 17, 9–16.

Wang, Y., Xue, P., and Wang, J. (2011). Comparing study of energy-absorbing behavior for honeycomb structures. *Key Eng. Mater.* 462-463, 13–17.

Yang, C., Vora, H. D., and Chang, Y. (2018). Behavior of auxetic structures under compression and impact forces. *Smart Mater. Struct.* 27, 025012.

Yao, T., Deng, Z., Zhang, K., and Li, S. (2019). A method to predict the ultimate tensile strength of 3D printing polylactic acid (PLA) materials with different printing orientations. *Compos. Part B Eng.* 163, 393–402.

Yeoh, C. K., Cheah, C. S., Pushpanathan, R., Song, C. C., Tan, M. A., and Teh, P. L. (2020). Effect of infill pattern on mechanical properties of 3D printed PLA and cPLA. *IOP Conf. Ser. Mater. Sci. Eng.* 957, 012064.